INTERNATIONAL JOURNAL FOR NUMERICAL METHODS IN FLUIDS
Int. J. Numer. Meth. Fluids 2007; **54**:333–352
Published online 7 December 2006 in Wiley InterScience (www.interscience.wiley.com). DOI: 10.1002/fld.1413

Computation of 2D Navier–Stokes equations with moving interfaces by using GMRES

Jin Wang*, †

Department of Mathematics, Duke University, Box 90320, Durham, NC 27708, U.S.A.

SUMMARY

In this paper, we present a novel numerical algorithm to compute two-dimensional (2D) viscous interfacial flows governed by the incompressible Navier–Stokes equations together with interfacial conditions. The essential idea is to use the generalized minimum residual (GMRES) method to efficiently solve the large algebraic system resulting from the temporal and spatial discretizations. With this algorithm, moving interfaces can be captured with high accuracy and viscous effects on wave motion can be studied in detail.

Received 9 January 2006; Revised 8 October 2006; Accepted 31 October 2006

KEY WORDS: GMRES; interfacial motion; viscous effects; standing waves

1. INTRODUCTION

Viscous flows with interfaces occur in a wide variety of physical phenomena. Mathematically, the motion is governed by the incompressible Navier–Stokes equations together with interfacial conditions. Although much success has been achieved on the numerical study of such problems [1–4], understanding of the fundamental physics involved, in particular, viscous effects, remains limited due to the non-linear phenomena implicit in both the fluid flows and interfacial wave evolution. The challenge in studying these effects numerically is the design of an algorithm which captures the evolving interface with high accuracy and without introducing numerical smoothing. Current methods, such as volume-of-fluid [5, 6] or level set [7–9], succeed primarily for motions where the fine-scale surface details are not important [10, 11]. Boundary integral methods [12, 13], on the other hand, can only be applied to inviscid flows. Therefore, these methods are not suitable for an accurate study of viscous effects on interfacial motion.

*Correspondence to: Jin Wang, Department of Mathematics, Duke University, Box 90320, Durham, NC 27708, U.S.A.
†E-mail: wang@math.duke.edu

Contract/grant sponsor: NSF; contract/grant number: DMS-0112759

In this paper, we present a new approach to simulate two-dimensional (2D) viscous interfacial flows which ensures a highly accurate representation for the interface. Clearly, only a finite region of the fluid surface can be studied and it is reasonable to assume the region is periodic in the horizontal direction. It is then natural to use a spectral representation for the surface and flow variables in the horizontal coordinate. As a result, the flow equations become a family of equations in time and the vertical coordinate. Good resolution near the surface can be achieved by introducing a new vertical coordinate whose origin lies on the surface. Then, we perform the temporal and spatial (vertical) discretizations to the full mapped equations, which results in a large and non-symmetric linear system with variable coefficients. The generalized minimum residual (GMRES) algorithm is applied to find the solutions.

The GMRES method is an efficient tool to solve large and non-symmetric linear systems. This method was proposed by Saad and Schultz in 1986 [14] and its basic idea is as follows. Suppose we want to solve a linear system

$$Ax = b \tag{1}$$

where A is a non-singular $n \times n$ complex matrix and b a vector of length n. Let x_0 be an initial guess for this linear system and $r_0 = b - Ax_0$ be its corresponding residual. The GMRES algorithm builds an approximation to the solution of (1) in the form

$$x_m = x_0 + Q_m y \tag{2}$$

Here Q_m is an orthonormal basis for the Krylov subspace

$$\mathscr{K}(A, r_0, m) = \text{span}\{r_0, Ar_0, \ldots, A^{m-1}r_0\} \tag{3}$$

and is constructed *via* the Arnoldi process [15]. The vector y in Equation (2) is determined so that the L_2-norm of the residual $r_m = b - Ax_m$ is minimal over $\mathscr{K}(A, r_0, m)$. Usually one can use the Givens rotations [15] to solve for y. In practical application, GMRES requires some preconditioning to reduce the number of iterations and improve the efficiency of the algorithm [16]. We will describe the details of the GMRES implementation in the design of our numerical methods.

The outline of the paper is as follows. First, we present the 2D fluid equations in the mapped coordinates. Then, we describe the numerical discretizations for the temporal and spatial derivatives, followed by a detailed discussion of the GMRES iterations. Finally, we present the numerical results in both the validation of the accuracy of our numerical methods and the study of viscous effects on the motion of standing waves.

2. MAPPED EQUATIONS

Let us denote the spatial coordinates by (x, z), the temporal coordinate by t, the velocity components by (u, w) and the pressure by p. In addition, let the physical parameters ρ, μ, ν, g and γ be the density, the dynamic viscosity, kinematic viscosity, gravity and the surface tension coefficient, respectively.

DOI: 10.1002/fld

The equations of motion, in each of the two fluids, are given by the standard Navier–Stokes equations [17]

$$\rho u_t + \rho u u_x + \rho w u_z = -P_x + \mu(u_{xx} + u_{zz}) \tag{4}$$

$$\rho w_t + \rho u w_x + \rho w w_z = -P_z + \mu(w_{xx} + w_{zz}) \tag{5}$$

where P is the hydrodynamic pressure which includes the gravity, $P = p + \rho g z$. The incompressibility condition is

$$u_x + w_z = 0 \tag{6}$$

Equations (4)–(6) hold in both the upper and lower fluids. Their solutions are connected through the interfacial conditions. Let us represent the interface in the form

$$(x, z) = (x, h(x, t)) \tag{7}$$

Then h is determined by the kinematic condition

$$h_t + u^{(I)} h_x = w^{(I)} \tag{8}$$

where $u^{(I)}, w^{(I)}$ are the velocity components at the interface. Continuity of the velocity at the interface gives

$$u^{(1)} = u^{(2)} = u^{(I)}, \quad w^{(1)} = w^{(2)} = w^{(I)} \tag{9}$$

where the superscripts (1), (2) distinguish the upper and lower domains. Moreover, we have two stress conditions, or dynamical interfacial conditions

$$\begin{aligned}(h_x^2 - 1)[\mu^{(1)}(u_z^{(1)} + w_x^{(1)}) - \mu^{(2)}(u_z^{(2)} + w_x^{(2)})] \\ + 2h_x[\mu^{(1)}(u_x^{(1)} - w_z^{(1)}) - \mu^{(2)}(u_x^{(2)} - w_z^{(2)})] = 0\end{aligned} \tag{10}$$

$$\begin{aligned}(P^{(1)} - P^{(2)}) - gh(\rho^{(1)} - \rho^{(2)}) - 2[\mu^{(1)} w_z^{(1)} - \mu^{(2)} w_z^{(2)}] \\ + h_x[\mu^{(1)}(u_z^{(1)} + w_x^{(1)}) - \mu^{(2)}(u_z^{(2)} + w_x^{(2)})] - \gamma\kappa = 0\end{aligned} \tag{11}$$

where κ is the mean curvature of the interface

$$\kappa = \frac{h_{xx}}{(1 + h_x^2)^{3/2}} \tag{12}$$

Solutions are assumed to be smooth and 2π-periodic in the horizontal direction, and decay away from the interface in the vertical direction.

In order to capture the evolving interface with high resolution, we introduce the new, logical coordinates (X, Z, τ) through the mapping

$$x = X \tag{13}$$

$$z = F(X, Z, \tau) \tag{14}$$

$$t = \tau \tag{15}$$

DOI: 10.1002/fld

where

$$F(X, Z, \tau) \triangleq \begin{cases} Z + h(X, \tau)\exp(-\alpha Z), & Z \geqslant 0 \\ Z + h(X, \tau)\exp(\alpha Z), & Z \leqslant 0 \end{cases} \tag{16}$$

where $\alpha > 0$ is a constant. Clearly, when $Z = 0$, $z = h(x, t)$ marks the location of the interface. When far from the interface, Z is relaxing exponentially to z. The value of α can also be used to adjust the grid spacing near the interface.

We define

$$\begin{gathered} G_0 = \frac{F_\tau}{F_Z}, \quad G_1 = \frac{F_X}{F_Z}, \quad G_3 = \frac{1}{F_Z} \\ g_2 = (G_1)^2 + (G_3)^2, \quad g_3 = -2G_1, \quad g_4 = G_1\frac{\partial G_1}{\partial Z} + G_3\frac{\partial G_3}{\partial Z} - \frac{\partial G_1}{\partial X} \end{gathered} \tag{17}$$

Then we can write the Laplacian in new variables as

$$\mathscr{L} \triangleq \frac{\partial^2}{\partial x^2} + \frac{\partial^2}{\partial z^2} = \frac{\partial^2}{\partial X^2} + g_2\frac{\partial^2}{\partial Z^2} + g_3\frac{\partial^2}{\partial X \partial Z} + g_4\frac{\partial}{\partial Z} \tag{18}$$

Furthermore, we introduce a new variable q by

$$q = u_Z \tag{19}$$

Then the original equations (4)–(6) become

$$u_\tau - G_0 q + u(u_X - G_1 q) + wG_3 q = -\frac{1}{\rho}P_X + \frac{1}{\rho}G_1 P_Z + \nu\mathscr{L}\{u\} \tag{20}$$

$$w_\tau - G_0 w_Z + u(w_X - G_1 w_Z) + wG_3 w_Z = -\frac{1}{\rho}G_3 P_Z + \nu\mathscr{L}\{w\} \tag{21}$$

$$u_X - G_1 q + G_3 w_Z = 0 \tag{22}$$

where

$$\mathscr{L}\{u\} = u_{XX} + g_2 q_Z + g_3 q_X + g_4 q \tag{23}$$

and

$$\begin{aligned} \mathscr{L}\{w\} &= w_{XX} + g_2 w_{ZZ} + g_3 w_{XZ} + g_4 w_Z \\ &= w_{XX} - \frac{1}{G_3}[g_2(q_X - (G_1)_Z q) + g_3(u_{XX} - (G_1)_X q - G_1 q_X)] \\ &\quad - \left[\frac{1}{G_3}(g_2(G_3)_Z + g_3(G_3)_X) - g_4\right] w_Z + \frac{G_1}{G_3}g_2 q_Z \end{aligned} \tag{24}$$

DOI: 10.1002/fld

In deriving (24), we have used the equalities

$$w_{XZ} = -\frac{1}{G_3}[u_{XX} - (G_1)_X q - G_1 q_X + (G_3)_X w_Z] \tag{25}$$

$$w_{ZZ} = -\frac{1}{G_3}[q_X - (G_1)_Z q - G_1 q_Z + (G_3)_Z w_Z] \tag{26}$$

which can be obtained by differentiating (22) for X and Z, respectively.

Similarly, the stress conditions (10) and (11) are transformed to

$$\mu^{(1)}(G_3^{(1)} q^{(1)} + w_X^{(1)}) - \mu^{(2)}(G_3^{(2)} q^{(2)} + w_X^{(2)}) + \left(\frac{4h_X}{h_X^2 - 1} + \frac{G_1^{(1)}}{G_3^{(1)}}\right)\mu^{(1)}(u_X^{(1)} - G_1^{(1)} q^{(1)})$$

$$-\left(\frac{4h_X}{h_X^2 - 1} + \frac{G_1^{(2)}}{G_3^{(2)}}\right)\mu^{(2)}(u_X^{(2)} - G_1^{(2)} q^{(2)}) = 0 \tag{27}$$

$$(P^{(1)} - P^{(2)}) + \left(2 - \frac{4h_X^2}{h_X^2 - 1}\right)[\mu^{(1)}(u_X^{(1)} - G_1^{(1)} q^{(1)}) - \mu^{(2)}(u_X^{(2)} - G_1^{(2)} q^{(2)})]$$

$$- gh(\rho^{(1)} - \rho^{(2)}) - \gamma\kappa = 0 \tag{28}$$

There are no changes to the other two interfacial conditions (9). Now all the derivatives with respect to Z are first-order in the governing equations (19)–(22) as well as the interfacial conditions (27) and (28). This property is important in the design of our numerical methods.

3. NUMERICAL ALGORITHM

Based on the mapped equations, we develop our numerical algorithm as follows: the Crank–Nicolson method [18] is applied to the diffusion terms and the Adams–Bashforth method [19] to the advection terms to advance the solution in time. The discrete Fourier transform [20] is applied along the horizontal direction, X, which is assumed to possess periodicity. Then we obtain a first-order ordinary differential equation (ODE) system with respect to Z, the vertical coordinate. The trapezoidal rule is applied to this ODE system which results in a linear system of algebraic equations, where the coefficient matrix is large and has variable entries. We will use the GMRES method [14–16] to solve the linear system at each time step.

3.1. Temporal and spatial discretizations

Let us consider the details of the approximation in time. Denote the numerical solution at the nth time step by

$$(u^n, q^n, w^n, P^n, h^n)$$

DOI: 10.1002/fld

Suppose we know the numerical solution at the time steps $n-1$ and n, and we want to advance the solution to the next time step $n+1$. First, we update the interface h by applying the Adams–Bashforth method to Equation (8)

$$\frac{h^{n+1}-h^n}{\Delta\tau}=\frac{3}{2}(w^{(I)}-u^{(I)}h_X)^n-\frac{1}{2}(w^{(I)}-u^{(I)}h_X)^{n-1} \tag{29}$$

Once h^{n+1} is known, the mapping (13)–(15) is evaluated and the associated coefficients $G_i(i=0,1,3)$, g_i $(i=2,3,4)$ are readily calculated at the time step $n+1$. Then, by using the Crank–Nicolson method for the linear terms and the Adam–Bashforth method for the non-linear terms in Equations (20) and (21), we obtain

$$\begin{aligned}&\frac{u^{n+1}-u^n}{\Delta\tau}-\frac{1}{2}[(G_0q)^{n+1}+(G_0q)^n]\\&+\frac{3}{2}[u(u_X-G_1q)+wG_3q]^n-\frac{1}{2}[u(u_X-G_1q)+wG_3q]^{n-1}\\&=\frac{1}{2}\left[-\frac{1}{\rho}P_X+\frac{1}{\rho}G_1P_Z+v\mathscr{L}\{u\}\right]^{n+1}+\frac{1}{2}\left[-\frac{1}{\rho}P_X+\frac{1}{\rho}G_1P_Z+v\mathscr{L}\{u\}\right]^n\end{aligned} \tag{30}$$

$$\begin{aligned}&\frac{w^{n+1}-w^n}{\Delta\tau}-\frac{1}{2}[(G_0w_Z)^{n+1}+(G_0w_Z)^n]\\&+\frac{3}{2}[u(w_X-G_1w_Z)+wG_3w_Z]^n-\frac{1}{2}[u(w_X-G_1w_Z)+wG_3w_Z]^{n-1}\\&=\frac{1}{2}\left[-\frac{1}{\rho}G_3P_Z+v\mathscr{L}\{w\}\right]^{n+1}+\frac{1}{2}\left[-\frac{1}{\rho}G_3P_Z+v\mathscr{L}\{w\}\right]^n\end{aligned} \tag{31}$$

Equations (19) and (22) are evaluated at the time step $n+1$. By substituting (23) and (24) into (30) and (31) and rearranging terms, we obtain

$$u_Z^{n+1}=q^{n+1} \tag{32}$$

$$\frac{1}{2\rho}G_1^{n+1}P_Z^{n+1}+\frac{v}{2}g_2^{n+1}q_Z^{n+1}=U^{n+1}+E \tag{33}$$

$$G_3^{n+1}w_Z^{n+1}=-u_X^{n+1}+G_1^{n+1}q^{n+1} \tag{34}$$

$$\begin{aligned}&-\frac{1}{2\rho}G_3^{n+1}P_Z^{n+1}+\left[\frac{1}{2}G_0+\frac{v}{2}g_4-\frac{v}{2}\frac{1}{G_3}(g_2(G_3)_Z+g_3(G_3)_X)\right]^{n+1}w_Z^{n+1}\\&+\frac{v}{2}\left(\frac{G_1}{G_3}g_2\right)^{n+1}q_Z^{n+1}=V^{n+1}+F\end{aligned} \tag{35}$$

DOI: 10.1002/fld

where

$$U^{n+1}=\frac{u^{n+1}}{\Delta\tau}-\frac{1}{2}(G_0q)^{n+1}-\frac{1}{2}\left[-\frac{1}{\rho}P_X+\nu(u_{XX}+g_3q_X+g_4q)\right]^{n+1} \tag{36}$$

$$V^{n+1}=\frac{w^{n+1}}{\Delta\tau}-\frac{\nu}{2}\left\{w_{XX}-\frac{1}{G_3}[g_2(q_X-(G_1)_Zq)+g_3(u_{XX}-(G_1)_Xq-G_1q_X)]\right\}^{n+1} \tag{37}$$

and where E, F denote the explicit terms

$$\begin{aligned}E=&-\frac{u^n}{\Delta\tau}-\frac{1}{2}(G_0\,q)^n\\&+\frac{3}{2}[u(u_X-G_1q)+wG_3q]^n-\frac{1}{2}[u(u_X-G_1q)+wG_3q]^{n-1}\\&-\frac{1}{2}\left[-\frac{1}{\rho}P_X+\frac{1}{\rho}G_1P_Z+\nu(u_{XX}+g_2q_Z+g_3q_X+g_4q)\right]^n\end{aligned} \tag{38}$$

$$\begin{aligned}F=&-\frac{w^n}{\Delta\tau}-\frac{1}{2}(G_0\,w_Z)^n\\&+\frac{3}{2}[u(w_X-G_1w_Z)+wG_3w_Z]^n-\frac{1}{2}[u(w_X-G_1w_Z)+wG_3w_Z]^{n-1}\\&-\frac{1}{2}\left\{-\frac{1}{\rho}G_3P_Z+\nu\left[w_{XX}-\frac{1}{G_3}[g_2(q_X-(G_1)_Zq)+g_3(u_{XX}-(G_1)_Xq\right.\right.\\&\left.\left.-G_1q_X)]-\left[\frac{1}{G_3}(g_2(G_3)_Z+g_3(G_3)_X)-g_4\right]w_Z+\frac{G_1}{G_3}g_2q_Z\right]\right\}^n\end{aligned} \tag{39}$$

Now that Equations (32)–(35) involve only first-order derivatives terms with respect to Z, we apply the trapezoidal rule in Z to obtain

$$\frac{u_{j+1}^{n+1}-u_j^{n+1}}{\Delta Z}-\frac{1}{2}(q_{j+1}^{n+1}+q_j^{n+1})=0 \tag{40}$$

$$\begin{aligned}&\frac{1}{2\rho}(G_1^{n+1})_{j+1/2}\frac{P_{j+1}^{n+1}-P_j^{n+1}}{\Delta Z}+\frac{\nu}{2}(g_2^{n+1})_{j+1/2}\frac{q_{j+1}^{n+1}-q_j^{n+1}}{\Delta Z}\\&-\frac{(U^{n+1})_{j+1}+(U^{n+1})_j}{2}=\frac{E_{j+1}+E_j}{2}\end{aligned} \tag{41}$$

$$\begin{aligned}&(G_3^{n+1})_{j+1/2}\frac{w_{j+1}^{n+1}-w_j^{n+1}}{\Delta Z}+\frac{1}{2}[(u_X^{n+1})_{j+1}+(u_X^{n+1})_j]\\&-\frac{1}{2}[(G_1^{n+1}q^{n+1})_{j+1}+(G_1^{n+1}q^{n+1})_j]=0\end{aligned} \tag{42}$$

DOI: 10.1002/fld

$$-\frac{1}{2\rho}(G_3^{n+1})_{j+1/2}\frac{P_{j+1}^{n+1}-P_j^{n+1}}{\Delta Z}+\frac{v}{2}\left(\frac{G_1}{G_3}g_2\right)_{j+1/2}^{n+1}\frac{q_{j+1}^{n+1}-q_j^{n+1}}{\Delta Z}$$

$$+\left[\frac{1}{2}G_0+\frac{v}{2}g_4-\frac{v}{2}\frac{1}{G_3}(g_2(G_3)_Z+g_3(G_3)_X)\right]_{j+1/2}^{n+1}\frac{w_{j+1}^{n+1}-w_j^{n+1}}{\Delta Z}$$

$$-\frac{(V^{n+1})_{j+1}+(V^{n+1})_j}{2}=\frac{F_{j+1}+F_j}{2} \tag{43}$$

where the subscripts j, $j+1$ refer to the jth and $(j+1)$th grid points in the vertical direction, while the $j+1/2$ refers to the average over the grid points j and $j+1$. We note that all the terms on the left-hand sides of the above equations are evaluated at $t=(n+1)\Delta t$ with the superscript $n+1$ and all the terms on the right-hand sides are evaluated at previous times with superscripts n or $n-1$. We have yet to perform a discretization in the X direction, where the Fourier transform will be used to achieve spectral accuracy. Since the coefficients in the above equations, such as G_0, G_1, G_3, g_2, g_3, g_4, all depend on X, direct application of the discrete Fourier transform to any product with these coefficients will require the convolution rule and make the results far too complicated. Fortunately, the GMRES method does not require the explicit structure of the iteration matrix [16]. This enables us to apply the pseudo-spectral approach [20] to Equations (40)–(43) to obtain a linear algebraic system for each Fourier mode k

$$A_k\mathscr{Y}_k=S_k \tag{44}$$

where the unknown, $\mathscr{Y}_k$, is composed of the kth Fourier coefficients of u, q, w and P at all the vertical positions, and where the right-hand side vector S_k comes from the kth Fourier coefficients of the right-hand sides in Equations (40)–(43).

3.2. The GMRES iterations

We use the GMRES method to solve Equation (44). The main parts in performing a GMRES iteration are as follows:

(1) Calculate the right-hand side vector S_k, which we have discussed in detail.
(2) Make an initial guess for the solutions.
(3) Apply the preconditioner.
(4) Use the pseudo-spectral approach to perform the matrix–vector multiplication.

It is relatively easy to perform the matrix–vector multiplication, say $A_k\widetilde{Y}$. This is achieved by substituting a vector $\widetilde{Y}$ into the left-hand sides of Equations (40)–(43) and applying the pseudo-spectral approach. As a result, we obtain the right-hand sides corresponding to that vector $\widetilde{Y}$ and they give exactly $A_k\widetilde{Y}$. Note that the interfacial conditions (9), (27) and (28) are also included in the calculation with the pseudo-spectral approach. These conditions are evaluated at $t=(n+1)\Delta t$ and $Z=0$. That means they are treated implicitly.

Now we write out the details for making the initial guess. Let us go back to system (32)–(35). We linearize all the expressions evaluated at $t=(n+1)\Delta t$ (i.e. with superscripts $n+1$) so that the coefficients are approximated by

$$G_0=0,\quad G_1=0,\quad G_3=1,\quad g_2=1,\quad g_3=0,\quad g_4=0 \tag{45}$$

DOI: 10.1002/fld

We are led to an approximate system

$$u_Z^{n+1} = q^{n+1} \tag{46}$$

$$\frac{v}{2} q_Z^{n+1} = \frac{u^{n+1}}{\Delta\tau} + \frac{1}{2\rho} P_X^{n+1} - \frac{v}{2} u_{XX}^{n+1} + E \tag{47}$$

$$w_Z^{n+1} = -u_X^{n+1} \tag{48}$$

$$-\frac{1}{2\rho} P_Z^{n+1} = \frac{w^{n+1}}{\Delta\tau} + \frac{v}{2} q_X^{n+1} - \frac{v}{2} w_{XX}^{n+1} + F \tag{49}$$

Then we perform the Fourier transform in X on the above Equations (46)–(49), which yields the following ODE system for each Fourier mode k

$$\frac{\mathrm{d}}{\mathrm{d}Z} Y_k = B_k Y_k + R_k \tag{50}$$

where

$$B_k \triangleq \begin{bmatrix} 0 & 1 & 0 & 0 \\ \dfrac{1}{v\Delta\tau}(2 + vk^2\Delta\tau) & 0 & 0 & \dfrac{1}{\rho v}\mathrm{i}k \\ -\mathrm{i}k & 0 & 0 & 0 \\ 0 & -\rho v \mathrm{i}k & -\dfrac{\rho}{\Delta\tau}(2 + vk^2\Delta\tau) & 0 \end{bmatrix} \tag{51}$$

and

$$Y_k \triangleq \begin{pmatrix} u_k^{n+1} \\ q_k^{n+1} \\ w_k^{n+1} \\ P_k^{n+1} \end{pmatrix}, \quad R_k \triangleq \begin{pmatrix} 0 \\ \dfrac{2}{v} E_k \\ 0 \\ -2\rho F_k \end{pmatrix} \tag{52}$$

As before, the subscript k refers to the kth Fourier coefficient of the corresponding physical variable.

We also linearize the interfacial conditions (9), (27) and (28) to obtain

$$u^{(1)} - u^{(2)} = 0 \tag{53}$$

$$\mu^{(1)}(q^{(1)} + w_X^{(1)}) - \mu^{(2)}(q^{(2)} + w_X^{(2)}) = 0 \tag{54}$$

$$w^{(1)} - w^{(2)} = 0 \tag{55}$$

$$(P^{(1)} - P^{(2)}) + 2(\mu^{(1)} u_X^{(1)} - \mu^{(2)} u_X^{(2)}) = gh(\rho^{(1)} - \rho^{(2)}) + \gamma h_{XX} \tag{56}$$

DOI: 10.1002/fld

After the Fourier transform is applied, the above equations can be written as

$$I_k^{(1)} Y_k^{(1)} - I_k^{(2)} Y_k^{(2)} = r_k \tag{57}$$

where

$$I_k \triangleq \begin{bmatrix} 1 & 0 & 0 & 0 \\ 0 & \mu & \mathrm{i}k\mu & 0 \\ 0 & 0 & 1 & 0 \\ 2\mathrm{i}k\mu & 0 & 0 & 1 \end{bmatrix}, \quad r_k \triangleq \begin{pmatrix} 0 \\ 0 \\ 0 \\ (g(\rho^{(1)} - \rho^{(2)}) - k^2\gamma)h_k \end{pmatrix} \tag{58}$$

The ODE system (50) has to be solved subject to the interfacial conditions (57). We observe that the matrix B_k in (51) has four distinct eigenvalues

$$\lambda_1 = k, \quad \lambda_2 = -k, \quad \lambda_3 = \sqrt{k^2 + \frac{2}{\nu\Delta\tau}}, \quad \lambda_4 = -\sqrt{k^2 + \frac{2}{\nu\Delta\tau}} \tag{59}$$

We can use their associated eigenvectors to diagonalize the ODE system (50). The diagonalized system is reduced to four scalar linear equations and its solutions can be easily constructed. We then transform them back to obtain the solutions for the original system (50). These solutions Y_k, obtained for all the vertical points, will serve as the initial guess for GMRES.

Fortunately, the preconditioner works in the same way as making the initial guess, except that the right-hand side vectors R_k in (50) and r_k in (57) are different. They are the residuals in the iteration and are provided by GMRES. We simply substitute them into (50) and (57) and apply the procedure described above to construct the solutions.

In our numerical simulation, we set the stopping criterion of the iterations to be $\varepsilon < 10^{-9}$, where ε is the normwise backward error [16, 21] and is defined to be the ratio of the L_2-norm of the residue and that of the approximate solution. We found the GMRES typically requires 6–10 iterations at each time step to achieve convergence.

4. NUMERICAL RESULTS

4.1. Numerical verification of accuracy

While there is no doubt about the spectral accuracy in the X-direction where the discrete Fourier transform is applied to smooth functions, the order of accuracy for the time marching and the discretization in the Z-direction is to be justified by numerical experiments. Two examples serve for that purpose. These tests are performed on a 2.4 GHz Xeon dual-processor workstation.

In the first example, we consider the incompressible Navier–Stokes equations (4)–(6) with the exact solutions

$$\begin{aligned} u &= t\sin(2x)\mathrm{e}^{-2z} \\ w &= t\cos(2x)\mathrm{e}^{-2z} \\ P &= \frac{\rho}{2}(\cos(2x)\mathrm{e}^{-2z} - t^2\mathrm{e}^{-4z}) \end{aligned} \tag{60}$$

DOI: 10.1002/fld

which are exponentially decaying in the vertical direction and periodic in the horizontal direction. The spatial domain is defined as

$$\{(x, z)|0\leqslant x\leqslant 2\pi, h(x, t)\leqslant z\leqslant 4\} \tag{61}$$

where h, the bottom, is artificially set as

$$h(x, t) = 0.2\sin(x - t) \tag{62}$$

Only one fluid is concerned and there is actually no interface. Nevertheless, when applying our methods the wavy boundary $h(x, t)$ serves as the 'interface', on which the mapping (13)–(15) is readily formed (for $Z\geqslant 0$ only) and all the parts in our approach are readily applied. That means the mapped fluid equations and their numerical approximations will be thoroughly tested. On the other hand, the numerical treatment of the interfacial conditions will not be tested. The initial and the boundary values for u, w, P are taken from the exact solution (60).

We perform the computation for $\rho = 1$, $\mu = 0.313$ (corresponding to a Reynolds number $Re \doteq 100$) and run the codes until $t = 0.2$. We use 32 points in the X-direction so that the errors associated with ΔX is much smaller than those associated with Δt and ΔZ. Let N be the number of time steps and J the number of points in the Z-direction. We keep doubling N and J to check the error pattern. The results are presented in Table I, where $E(u, N, J)$ denotes the L_2-norm of the errors for u with the resolution of N time steps and J points in the Z-direction, and where $R(u, N, J)$ denotes the quantity

$$\sqrt{\frac{E(u, N/2, J/2)}{E(u, N, J)}}$$

Similar notations hold for $E(w, N, J)$, $R(w, N, J)$ and $E(P, N, J)$, $R(P, N, J)$. The results clearly indicate the second-order convergence in both Δt and ΔZ.

Table I. Numerical errors for the first test case, where the non-linear motion (60) in a one-fluid domain is calculated.

N	J	$E(u, N, J)$ ($R(u, N, J)$)	$E(w, N, J)$ ($R(w, N, J)$)	$E(P, N, J)$ ($R(P, N, J)$)
80	80	1.749×10^{-5} (—)	8.921×10^{-6} (—)	5.487×10^{-5} (—)
160	160	4.555×10^{-6} (1.96)	2.130×10^{-6} (2.05)	1.302×10^{-5} (2.05)
320	320	1.143×10^{-6} (2.00)	5.554×10^{-7} (1.96)	3.403×10^{-6} (1.96)

N and J are the numbers of time steps and spatial points, respectively. $E(\cdot, N, J)$ denotes the L_2-norm of the errors and $R(\cdot, N, J)$ indicates the order of convergence.

DOI: 10.1002/fld

In the second example, we test a two-fluid case with an interface. Due to the presence of the non-linear interfacial conditions (9)–(11), an analytical form of solutions is generally not available. Instead, we consider the linearized problem, where the exact solutions are known, and we numerically calculate such solutions. Consequently, the numerical treatment of the interfacial conditions will be tested at least at the linear level.

Solutions for the linear motion of interfacial flows are available in [22] and most recently in [23]. They take the form of

$$\begin{pmatrix} u_k \\ w_k \\ P_k \\ h_k \end{pmatrix} = \begin{pmatrix} u_k^0 \\ w_k^0 \\ P_k^0 \\ h_k^0 \end{pmatrix} \mathrm{e}^{\sigma t} \tag{63}$$

where the subscript k specifies the kth Fourier coefficient and the superscript 0 indicates the initial state. The value of σ is found through a non-linear dispersion relation [22, 23] and Newton's method is applied to solve for σ numerically. Let $\Omega^{(1)} = \sqrt{\sigma + \nu^{(1)}k^2}$, $\Omega^{(2)} = \sqrt{\sigma + \nu^{(2)}k^2}$. The initial values $\{u_k^0, w_k^0, P_k^0, h_k^0\}$ are determined as follows.

In the upper domain

$$\begin{aligned} w_k^0 &= A\exp(-|k|z) + B\exp\left(-\frac{\Omega^{(1)}}{\sqrt{\nu^{(1)}}}z\right) \\ u_k^0 &= -\frac{\mathrm{i}|k|}{k}A\exp(-|k|z) - \frac{\mathrm{i}}{k}\frac{\Omega^{(1)}}{\sqrt{\nu^{(1)}}}B\exp\left(-\frac{\Omega^{(1)}}{\sqrt{\nu^{(1)}}}z\right) \\ P_k^0 &= \frac{\rho^{(1)}\sigma(k)}{|k|}A\exp(-|k|z) \end{aligned} \tag{64}$$

In the lower domain

$$\begin{aligned} w_k^0 &= C\exp(|k|z) + D\exp\left(\frac{\Omega^{(2)}}{\sqrt{\nu^{(2)}}}z\right) \\ u_k^0 &= \frac{\mathrm{i}|k|}{k}C\exp(|k|z) + \frac{\mathrm{i}}{k}\frac{\Omega^{(2)}}{\sqrt{\nu^{(2)}}}D\exp\left(\frac{\Omega^{(2)}}{\sqrt{\nu^{(2)}}}z\right) \\ P_k^0 &= -\frac{\rho^{(2)}\sigma(k)}{|k|}C\exp(|k|z) \end{aligned} \tag{65}$$

For the interface

$$h_k^0 = \frac{a}{2} \tag{66}$$

where a is a small real constant that specifies the amplitude. The constants A, B, C, D are given in [23].

DOI: 10.1002/fld

In our test we pick $k=1$, $a=0.4$ and consider the air–water case with $\rho^{(1)}=0.0012$, $\mu^{(1)}=1.8\times10^{-4}$, $\rho^{(2)}=1.0$, $\mu^{(2)}=1.1\times10^{-2}$ (corresponding to a Reynolds numbers $Re\doteq2846$). The domain of computation, with air above and water below, is chosen to be a rectangle

$$\{(x,z)|0\leqslant x\leqslant 2\pi,\ -H\leqslant z\leqslant H\} \tag{67}$$

with $H=4$. The initial conditions and the boundary values at the two ends ($z=\pm H$) are taken from the linear solutions. We advance the solution until $t=0.2$, using fixed 32 points in the X-direction, $2J$ points in the Z-direction and N steps in time. The results are shown in Table II, where the quantities E and R are defined as before. We see bigger numerical errors than those in the first test case. The reason is that in the present case, the viscosities are much smaller (i.e. the Reynolds numbers are much bigger), so that higher resolution is required to achieve good accuracy. Nevertheless, the results in the table clearly indicate the second-order convergence of the numerical methods. In particular, the interface profile, h, is captured with full second-order accuracy.

Further evidence of the accuracy and reliability of the numerical algorithm is provided in next section for the simulation of viscous effects on the motion of standing waves.

4.2. Numerical simulation of viscous standing waves

Two-dimensional standing waves in inviscid fluids are periodic in both time and space. They are stationary in the horizontal direction but make periodic oscillations between crest and trough in the vertical direction. The study of inviscid standing waves is an attractive topic in mathematical fluid mechanics and many efforts have been devoted to it. Rayleigh [24] was the first to investigate deep-water standing waves by calculating a perturbation series to the third order with the wave amplitude being the small parameter. Penney and Price [25] carried the perturbation series expansion to the fifth order. They found that the free surface is never perfectly flat during the period of the wave motion. By using digital computers to perform the coefficient arithmetic, Schwartz and Whitney [26] were able to compute the expansion to extremely high orders. In addition, Rottman [27]

Table II. Results for the second test case, where the linearized interfacial motion (63) between air and water is calculated.

N	J	$E(u,N,J)$ ($R(u,N,J)$)	$E(w,N,J)$ ($R(w,N,J)$)	$E(P,N,J)$ ($R(P,N,J)$)	$E(h,N,J)$ ($R(h,N,J)$)
80	80	2.747×10^{-2}	1.821×10^{-2}	3.328×10^{-1}	1.410×10^{-3}
		(—)	(—)	(—)	(—)
160	160	5.784×10^{-3}	4.372×10^{-3}	8.001×10^{-2}	3.250×10^{-4}
		(2.18)	(2.04)	(2.04)	(2.08)
320	320	1.293×10^{-3}	1.045×10^{-3}	2.104×10^{-2}	7.597×10^{-5}
		(2.11)	(2.05)	(1.95)	(2.06)

N and J are the numbers of time steps and spatial points, respectively. $E(\cdot,N,J)$ denotes the L_2-norm of the errors and $R(\cdot,N,J)$ indicates the order of convergence.

DOI: 10.1002/fld

computed high order series solutions for standing waves between two fluids with different but uniform densities. Further references on this topic can be found in the review article by Schwartz and Fenton [28].

On the other hand, relatively few work, in general, has ever been published for the viscous effects on the motion of finite amplitude waves. In the classical fluid dynamics book by Lamb [29], viscous theory was developed for linear wave motion at a one-fluid free surface. Chandrasekhar [22] extended the linear viscous theory to interfacial waves between two fluids. A recent paper by Yang and Tryggvason [30] investigated the effects of the viscosity on the motion of weakly non-linear progressive/travelling waves. They found, in the case of low Reynolds numbers, that wave profiles closely follow the linear prediction. A similar result was presented by Sussman in [9] where a level set method was used for the numerical simulation of waves.

In this section, we apply our numerical method to study the non-linear problem of standing wave motions in the presence of viscosity, by solving the fully non-linear Navier–Stokes equations with interfacial conditions.

We note that an inviscid standing wave can be expanded in a Fourier cosine series

$$h(x,t)=\sum_{k=1}^{\infty} A_k(A,t)\cos kx \tag{68}$$

where A is a free parameter and where each coefficient A_k is dependent on A and t. The expressions of the first few coefficients are given in [25], for example. In particular, when the wave is at its peak, the first five coefficients are given by

$$\begin{aligned} A_1 &= A+\tfrac{1}{32}A^3-\tfrac{47}{1344}A^5\\ A_2 &= \tfrac{1}{2}A^2-\tfrac{79}{672}A^4\\ A_3 &= \tfrac{3}{8}A^3-\tfrac{12563}{59136}A^5\\ A_4 &= \tfrac{1}{3}A^4\\ A_5 &= \tfrac{295}{768}A^5 \end{aligned} \tag{69}$$

At the initial moment, the wave is at its peak and the fluid is at rest, i.e. the velocities u and w are zero everywhere.

Since all fluids in nature have some viscosity, it is interesting to know what happens to a standing wave in the presence of viscosity. In order to numerically study this problem, we perform the simulation in the following way. We consider a system of two viscous fluids and use the expansion formula (69) for initial conditions. The numerical solution is recorded from time to time, in particular, at every period T when the wave attains its peak, and compared with the inviscid solution. We neglect the surface tension in this study.

There are two issues which we have to address for using such initial conditions. First, formula (69) is for a one-fluid system with the density of the upper fluid being zero, while our computation is for a two-fluid system with a non-zero upper density. According to [22, 30], a small upper density will contribute extra terms with a leading order $\rho^{(1)}/\rho^{(2)}\sqrt{Re}$. In our numerical simulation the density ratio $\rho^{(1)}/\rho^{(2)}$ is close to 10^{-3} and the Reynolds number Re is either about 3000 or 300. Hence, the error due to a non-zero upper density is negligible since it is at most in the magnitude of 10^{-5}. Second, formula (69) corresponds to inviscid solutions. As soon as the

DOI: 10.1002/fld

computation is started in the presence of viscosity, boundary layers form near the interface to ensure the velocities become continuous and the stresses become important in the balance of pressure across the interface. Numerically we found the effect of this spontaneous adjustment is very small and it only affects the fifth or sixth digits of the numerical results.

Figure 1 shows the wave profiles at $t=0$, with $A=0.1$, and $t=20T$, with two choices of viscosities: (1) The typical air–water case with $\rho^{(1)}=0.0012$, $\mu^{(1)}=1.8\times10^{-4}$, $\rho^{(2)}=1.0$, $\mu^{(2)}=1.1\times10^{-2}$. The Reynolds number $Re\doteq2846$. (2) An artificial case where the densities are the same with, but the viscosities are 10 times bigger than, the air–water case. Specifically, $\rho^{(1)}=0.0012$, $\mu^{(1)}=1.8\times10^{-3}$, $\rho^{(2)}=1.0$, $\mu^{(2)}=1.1\times10^{-1}$. The Reynolds number $Re\doteq285$. One can clearly see the decay of the wave amplitude. In the case of bigger viscosities (Figure 1(b)) the wave decays faster than in the air–water case (Figure 1(a)).

Before we explore more details of the viscous effects, we provide one more validation of our numerical methods by checking the accuracy in the calculation of the non-linear interface, h. This complements the second test for the numerical treatment of the full interfacial conditions. Due to the presence of viscosity, an exact solution of the interface profile is not known. Hence, we use the Richardson extrapolation [19] to check the order of accuracy. Let $\widehat{h}(N, J)$ be the numerical solution of h with N time steps and J points in the vertical direction. We define

$$e(N, J)=\|\widehat{h}(N/2, J/2)-\widehat{h}(N, J)\|_2, \quad r(N, J)=\sqrt{\frac{e(N/2, J/2)}{e(N, J)}}$$

where $\|\cdot\|_2$ denotes the L_2-norm taken at all the grid points in the horizontal direction. In our numerical test, we consider a system of air (upper fluid) and water (lower fluid) in a rectangular domain as defined in (67). We pick $H=16$, far bigger than the wave amplitude to ensure the far field boundaries have no impacts on the interfacial motion. Sufficiently many points are used in the horizontal direction so that the error associated with ΔX can be neglected. We advance the numerical solution until after six periods for each choice of N and J. The results are presented in Table III.

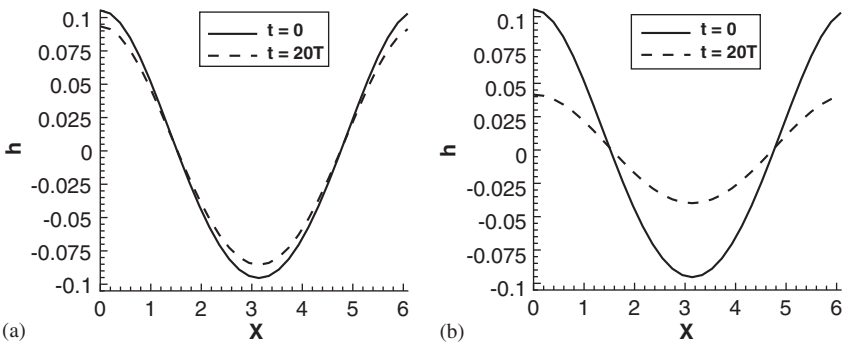

Figure 1. The profiles of standing waves in the presence of viscosity. The profiles at $t=0$ are from the analytic expansion form with $A=0.1$, and those at $t=20T$, where T is one wave period, are obtained from the numerical simulation: (a) in the air–water case: $\rho^{(1)}=0.0012$, $\mu^{(1)}=1.8\times10^{-4}$, $\rho^{(2)}=1.0$, $\mu^{(2)}=1.1\times10^{-2}$ and (b) with bigger viscosities: $\rho^{(1)}=0.0012$, $\mu^{(1)}=1.8\times10^{-3}$, $\rho^{(2)}=1.0$, $\mu^{(2)}=1.1\times10^{-1}$.

DOI: 10.1002/fld

Table III. Convergence study for the numerical calculation of the non-linear interface from a viscous standing wave between air and water.

N	J	$e(N, J)$	$r(N, J)$
160	160	—	—
320	320	1.495×10^{-3}	—
640	640	4.212×10^{-4}	1.88
1280	1280	8.860×10^{-5}	2.18

N and J are the numbers of time steps and spatial points, respectively. $e(N, J)$ denotes the L_2-norm of the difference between two consecutive numerical runs and $r(N, J)$ indicates the order of convergence.

The values of r indicate, again, the second-order accuracy in both t and Z. The results, together with those from the first two tests, give a solid validation of our numerical methods.

It is worthwhile to compare the accuracy of our numerical method with that of level set methods, which have been increasingly popular in the calculation of fluid interface problems. The level set algorithm, though robust and applicable in a wide range of problems, cannot in general achieve second-order accuracy for problems involving moving interfaces between two incompressible fluids [9]. In a very recent paper by Sussman *et al.* [31], a coupled level set and volume of fluid method was proposed which achieves second-order accuracy in the limit of zero upper density. This is a significant improvement of the level set algorithm in the calculation of two-phase flows. However, this method is of full second order only when the upper fluid vanishes. In the case of air and water with a density ratio 1 to 1000, the order of 1.6 was reported for the simulation of standing waves and only first order measured in the simulation of travelling waves with wind [31]. On the other hand, the main advantage of level set methods over our present method lies in its ability to easily handle topological changes of interfaces, though change in topology is not a concern in our study of the viscous effects on wave motions.

Now we discuss the main results of the numerical simulation of standing waves in the presence of viscosity. We have seen that the viscous dissipation damp the wave amplitude. It is then interesting to ask: in what pattern does the viscosity damp the wave amplitude? In particular, does the viscosity break a standing wave of the expansion form (68)? In order to answer the question, we study the decay pattern of each Fourier mode A_k in detail. For the inviscid case, the expansion formulas in (69) suggest one way to view the family of standing waves is to consider the curves A_k *versus* A_1, or equivalently, $A_k(A_1)$. Then the effects of viscosity can be studied by viewing the deviation of the numerical results from these curves.

We draw the curves by using (69) for the amplitude of the modes $|A_2|$ *versus* $|A_1|$, $|A_3|$ *versus* $|A_1|$, etc. and refer to these curves as inviscid solutions. On the other hand, we have the numerical results for the viscous solutions which give the time evolution for the amplitude of each mode. We can plot these amplitudes in the same way as $|A_2|$ *versus* $|A_1|$, $|A_3|$ *versus* $|A_1|$, etc. In Figures 2–4 we compare the viscous solutions, obtained numerically, to the analytic inviscid solutions with two choices of the amplitude parameter, $A = 0.1$ and 0.2. We again consider the two choices of viscosities: one in the air–water case and one with 10 times bigger viscosities.

The numerical solutions are plotted from $t = 0$ and for every period T, until $t = 20T$. In all these figures, we observe that the numerical viscous solutions (the squares) closely follow the analytical inviscid solutions (the curves). These results suggest that viscous effects simply reduce

DOI: 10.1002/fld

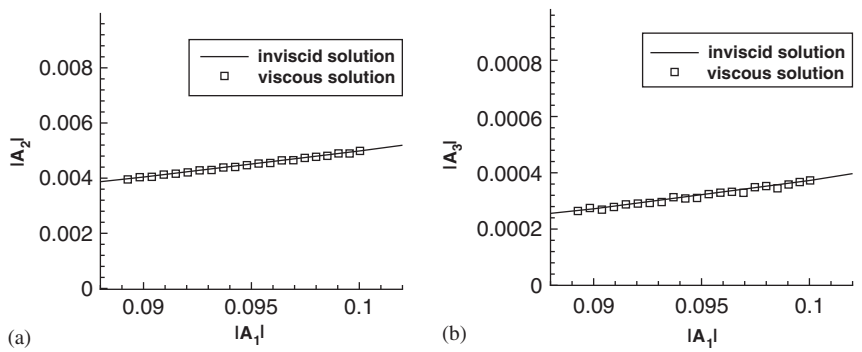

Figure 2. Comparison between the inviscid solution, obtained analytically, and the viscous solution, obtained numerically, of the standing wave with $\rho^{(1)} = 0.0012$, $\mu^{(1)} = 1.8 \times 10^{-4}$, $\rho^{(2)} = 1.0$, $\mu^{(2)} = 1.1 \times 10^{-2}$ and $A = 0.1$. The numerical solution is displayed from $t = 0$ and for every period, T, until $t = 20T$: (a) modes $|A_2|$ *versus* $|A_1|$ and (b) modes $|A_3|$ *versus* $|A_1|$.

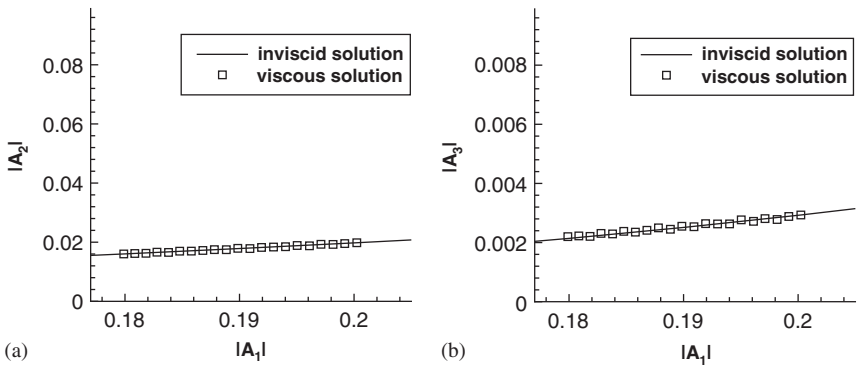

Figure 3. Comparison between the inviscid solution, obtained analytically, and the viscous solution, obtained numerically, of the standing wave with $\rho^{(1)} = 0.0012$, $\mu^{(1)} = 1.8 \times 10^{-4}$, $\rho^{(2)} = 1.0$, $\mu^{(2)} = 1.1 \times 10^{-2}$ and $A = 0.2$. The numerical solution is displayed from $t = 0$ and for every period, T, until $t = 20T$: (a) modes $|A_2|$ *versus* $|A_1|$ and (b) modes $|A_3|$ *versus* $|A_1|$.

the magnitude (peak value) of a standing wave while allowing it to remain a member of the family. In other words, the viscous dissipation seems to be equivalent to the damping of the amplitude parameter A in expansion (68). Without viscosity, A is fixed. With viscosity it is reduced while maintaining the ratio of the amplitudes between different modes.

One more evidence is provided in Figure 5, where we match the numerical solutions of viscous standing waves at $t = 20T$ by using some analytic solutions from inviscid standing waves. The air–water case is considered and two choices for the initial wave amplitude are made: $A = 0.1$ and 0.2. From the numerical solutions we are able to obtain the magnitude of the mode A_1 at $t = 20T$ in each case. From A_1 we can solve for A by using the first equation in (69). We then substitute A into the expansion (69) to obtain an inviscid solution. The numerical solutions and the inviscid solutions are plotted for both cases in Figure 5 and we find excellent agreement between them.

DOI: 10.1002/fld

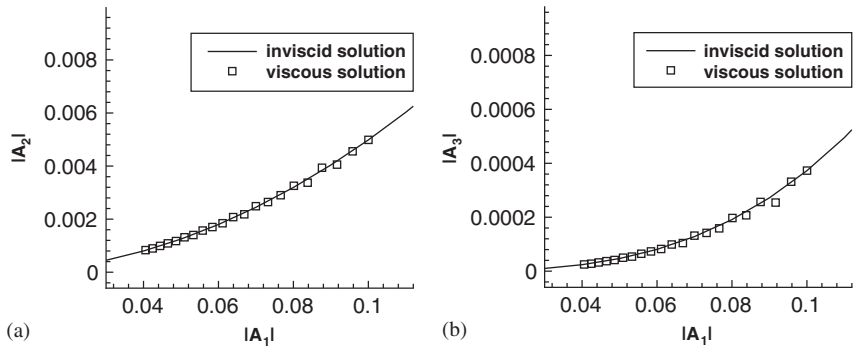

Figure 4. Comparison between the inviscid solution, obtained analytically, and the viscous solution, obtained numerically, of the standing wave with $\rho^{(1)} = 0.0012$, $\mu^{(1)} = 1.8 \times 10^{-3}$, $\rho^{(2)} = 1.0$, $\mu^{(2)} = 1.1 \times 10^{-1}$ and $A = 0.1$. The numerical solution is displayed from $t = 0$ and for every period, T, until $t = 20T$: (a) modes $|A_2|$ *versus* $|A_1|$ and (b) modes $|A_3|$ *versus* $|A_1|$.

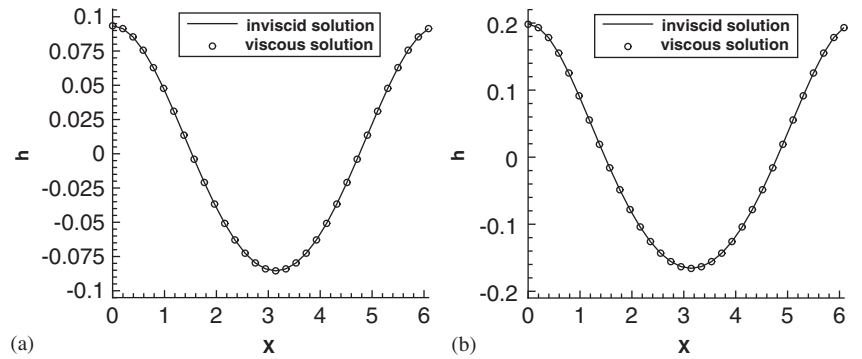

Figure 5. Matching the inviscid solution, obtained analytically, and the viscous solution, obtained numerically, for the profiles of standing waves with $\rho^{(1)} = 0.0012$, $\mu^{(1)} = 1.8 \times 10^{-4}$, $\rho^{(2)} = 1.0$, $\mu^{(2)} = 1.1 \times 10^{-2}$: (a) the numerical solution starts from $A = 0.1$ and is plotted at $t = 20T$, while the inviscid solution is plotted with $A \doteq 0.08916$ and (b) the numerical solution starts from $A = 0.2$ and is plotted at $t = 20T$, while the inviscid solution is plotted with $A \doteq 0.17972$.

Finally, we mention again that the surface tension is not included in our numerical study of standing waves. In the presence of capillary effects, waves will typically develop sharp corners at the top and bottom of the leading edge, which clearly breaks the pattern of standing waves. See [30, 32], for example, for detailed discussion of capillary effects on wave motion.

5. CONCLUSIONS

We have designed an algorithm which enables us to perform direct numerical simulation of two-dimensional Navier–Stokes equations with moving interfaces. The GMRES iterations play a crucial role in this algorithm and make it possible to efficiently solve the large linear system resulting from

DOI: 10.1002/fld

the temporal and spatial discretizations. The methods achieve spectral accuracy in the horizontal direction, and second-order accuracy in both the time marching and the vertical direction. With this numerical algorithm, standing waves can be followed sufficiently in time to study the viscous effects on wave motion. Our numerical results suggest, at least for standing waves with small or moderate amplitude, that viscous dissipation appears to be equivalent to the damping of the parameter A in the inviscid expansion form. This observation will be used to derive a formal asymptotic theory for further study of the viscous effects on standing waves.

ACKNOWLEDGEMENTS

The author would like to thank Greg Baker for many pleasant conversations during the preparation of this paper, and thank Tom Beale and Mark Sussman for helpful discussions. The author would also like to thank the referee for valuable suggestions. This work has been partially supported by NSF Grant no. DMS-0112759.

REFERENCES

1. Ferziger JH, Peric M. *Computational Methods for Fluid Dynamics*. Springer: Berlin, 2002.
2. Gent PR, Taylor PA. A numerical model of the air flow above water waves. *Journal of Fluid Mechanics* 1976; **77**:105–128.
3. Peyret R, Taylor TD. *Computational Methods for Fluid Flow*. Springer: Berlin, 1983.
4. Scardovelli R, Zaleski S. Direct numerical simulation of free surface and interfacial flow. *Annual Review of Fluid Mechanics* 1999; **31**:567–603.
5. Hirt CW, Nichols BD. Volume of fluid (VOF) method for dynamics of free boundaries. *Journal of Computational Physics* 1981; **39**:201–225.
6. Noh WF, Woodward PR. SLIC (simple line interface calculation). *Proceedings of the Fifth International Conference on Fluid Dynamics*. Lecture Notes in Physics, vol. 59. Springer: Berlin, 1976; 330–340.
7. Osher S, Sethian JA. Fronts propagating with curvature-dependent speed: algorithms based on Hamilton–Jacobi formulations. *Journal of Computational Physics* 1988; **79**:12–49.
8. Sethian JA. *Level Set Methods and Fast Marching Methods*. Cambridge University Press: Cambridge, MA, 2000.
9. Sussman M, Fatemi E, Smereka P, Osher S. An improved level set method for incompressible two-phase flows. *Computers and Fluids* 1998; **27**:663–680.
10. Chang YC, Hou TY, Merriaman B, Osher S. A level set formulation of Eulerian interface capturing methods for incompressible fluid flows. *Journal of Computational Physics* 1996; **124**:449–464.
11. Sethian JA, Smereka P. Level set methods for fluid interfaces. *Annual Review of Fluid Mechanics* 2003; **35**:341–372.
12. Baker GR, Meiron DI, Orszag SA. Generalized vortex methods for free surface flow problems. *Journal of Fluid Mechanics* 1982; **123**:477–501.
13. Beale JT. A convergent boundary integral method for three-dimensional water waves. *Mathematics of Computation* 2001; **70**:977–1029.
14. Saad Y, Schultz M. GMRES: a generalized minimal residual algorithm for solving non-symmetric linear systems. *SIAM Journal on Scientific and Statistical Computing* 1986; **7**:856–869.
15. Golub GH, Van Loan CF. *Matrix Computations*. The Johns Hopkins University Press: Baltimore, MD, 1996.
16. Fraysse V, Giraud L, Gratton S. A set of GMRES routines for real and complex arithmetics. *CERFACS Technical Report TR/PA/97/49*, France, 1997.
17. Batchelor GK. *An Introduction to Fluid Dynamics*. Cambridge University Press: Cambridge, 1967.
18. Richtmyer RD, Morton KW. *Difference Method for Initial Value Problems*. Wiley: New York, 1967.
19. Anderson DA, Tannehill JC, Pletcher RH. *Computational Fluid Mechanics and Heat Transfer*. Hemisphere Publishing Corporation: Washington, DC, 1984.
20. Peyret R. *Spectral Methods for Incompressible Flow*. Springer: Berlin, 2002.
21. Chaitin-Chatelin F, Fraysse V. *Lectures on Finite Precision Computations*. SIAM: Philadelphia, PA, 1996.
22. Chandrasekhar S. *Hydrodynamic and Hydromagnetic Stability*. Clarendon Press: Oxford, 1961.

DOI: 10.1002/fld

23. Baker GR, Wang J, Johnson JT, Hayslip AR. The linear stability at the interface between two immiscible incompressible fluids. In preparation.
24. Rayleigh JWS. Deep water waves, progressive or stationary, to the third order of approximation. *Proceedings of the Royal Society of London*, *Series A* 1915; **91**:345–353.
25. Penney WG, Price AT. Some gravity wave problems in the motion of perfect liquids. Part II: Finite periodic stationary gravity waves in a perfect liquid. *Philosophical Transactions of the Royal Society of London*, *Series A* 1952; **244**:251–284.
26. Schwartz LW, Whitney AK. A semi-analytic solution for nonlinear standing waves in deep water. *Journal of Fluid Mechanics* 1981; **107**:147–171.
27. Rottman JW. Steep standing waves at a fluid interface. *Journal of Fluid Mechanics* 1982; **124**:283–306.
28. Schwartz LW, Fenton JD. Strongly nonlinear waves. *Annual Review of Fluid Mechanics* 1982; **14**:39–60.
29. Lamb H. *Hydrodynamics*. Dover Publications: New York, 1945.
30. Yang Y, Tryggvason G. Dissipation of energy by finite-amplitude surface waves. *Computers and Fluids* 1998; **27**:829–845.
31. Sussman M, Smith KM, Hussaini MY, Ohta M, Zhi-Wei R. A sharp interface method for incompressible two-phase flows. *Journal of Computational Physics*. Available online 27 July 2006, in press.
32. Whitham GB. *Linear and Nonlinear Waves*. Wiley: New York, 1974.

DOI: 10.1002/fld